Letters

A Critical Examination of Frequency-Fixed Second-Order Generalized Integrator-Based Phase-Locked Loops

Saeed Golestan, *Senior Member, IEEE*, Seyyed Yousef Mousazadeh, Josep M. Guerrero, *Fellow, IEEE*, and Juan C. Vasquez, *Senior Member, IEEE*

***Abstract*—The implementation of a large number of single-phase phase-locked loops (PLLs) involves creating a fictitious quadrature signal. A popular approach for this purpose is using a second-order generalized integrator-based quadrature signal generator (SOGI-QSG) because it results in an acceptable speed/accuracy tradeoff. The SOGI-QSG-based PLL (or briefly the SOGI-PLL), in its standard form, involves a frequency feedback loop for adjusting the SOGI resonance frequency under frequency drifts. Some recent research works have reported that the speed/accuracy tradeoff of the SOGI-PLL can be considerably enhanced by removing the frequency feedback loop. In these methods, the SOGI resonance frequency is fixed at the nominal frequency, and a compensation strategy for correcting errors caused under off-nominal frequencies is employed. The main aim of this letter is to provide a critical analysis of frequency-fixed SOGI-based PLLs to highlight their real advantages and disadvantages.**

***Index Terms*—Quadrature signal generation (QSG), phase-locked loop (PLL), second-order generalized integrator (SOGI), synchronization.**

I. Introduction

In RECENT years, a large number of single-phase phase-locked loops (PLLs) have been proposed in the literature. Depending on their phase detector (PD), these PLLs can be categorized as power-based PLLs (pPLLs) and quadrature signal generation-based PLLs (QSG-PLLs) [1].

The standard pPLL uses a simple mixer as the PD [2]. This PD, nevertheless, results in a large double-frequency disturbance component, which causes offset and double-frequency oscillatory errors in the pPLL estimated quantities [1]. To address this problem, different filters such as a moving average filter, notch filter, or high-order low-pass filter can be included inside the control loop of the standard pPLL [1], [3]–[5]. Another approach is reconstructing and canceling the double-frequency disturbance term by using the estimated phase angle and amplitude [1], [6].

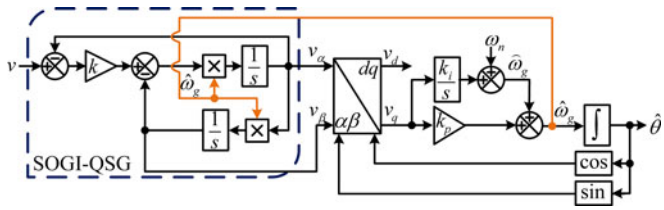

Fig. 1. Schematic diagram of the standard SOGI-PLL.

The QSG-PLLs are single-phase variants of the conventional synchronous reference frame PLL (SRF-PLL) [7]. The main difference of these PLLs is in the way they create the quadrature signal, which is required for transferring information into the *dq* frame. The transfer delay, all-pass filter, Kalman filter, differentiator, inverse Park transform, Hilbert transformer, sliding discrete Fourier transform, and generalized integrators are well-known algorithms/filters for generating the quadrature signal [1], [8].

Employing the second-order generalized integrator (SOGI) is one of the most popular approaches for creating the quadrature signal [9]. The schematic diagram of a single-phase PLL with the SOGI-based QSG can be observed in Fig. 1 [9], in which v is the single-phase input signal, $\hat{\theta}$ is the estimated phase angle, $\hat{\omega}_g$ and $\widehat{\omega}_g$ are both estimations for the grid frequency, ω_n is the nominal frequency, and k_p and k_i are the proportional and integral gains of the proportional-integral (PI) controller, respectively. This PLL structure is often referred to as the SOGI-PLL. The reported results demonstrate that a well-tuned SOGI-PLL can achieve a rather fast dynamic response and an acceptable harmonic filtering capability [8].

Recently, some attempts for enhancing the speed/accuracy tradeoff of the standard SOGI-PLL have been made by some researchers [10], [11]. To be more exact, it is recommended in [10] and [11] to remove the frequency feedback loop and use frequency-fixed SOGI(s) (FFSOGI) in combination with some compensation units in the PLL structure. It is claimed that the FFSOGI-based PLLs (FFSOGI-PLLs) provide a better performance than the standard SOGI-PLL [10], [11]. The main aim of this letter is to provide an analysis of FFSOGI-PLLs to highlight their real advantages and disadvantages.

Manuscript received December 21, 2016; revised January 16, 2017; accepted January 24, 2017. Date of publication February 24, 2017; date of current version April 24, 2017.

S. Golestan, J. M. Guerrero, and J. C. Vasquez are with the Department of Energy Technology, Aalborg University, Aalborg DK-9220, Denmark (e-mail: sgd@et.aau.dk; joz@et.aau.dk; juq@et.aau.dk).

S. Y. Mousazadeh is with the Department of Electrical Engineering, Iran University of Science and Technology, Tehran 13114-16846, Iran (e-mail: s_y_mosazade@iust.ac.ir).

Color versions of one or more of the figures in this letter are available online at http://ieeexplore.ieee.org.

Digital Object Identifier 10.1109/TPEL.2017.2674973

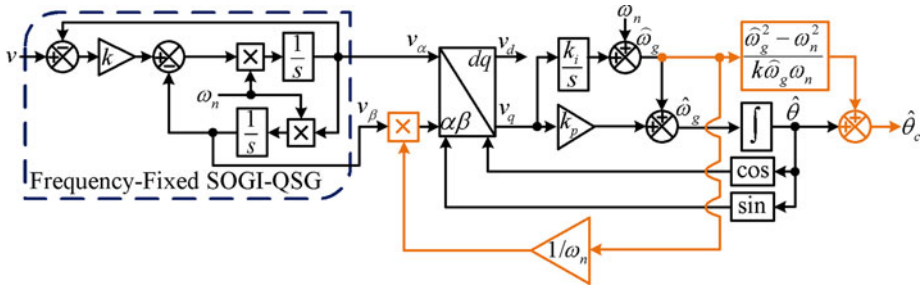

Fig. 2. Schematic diagram of the FFSOGI-PLL1.

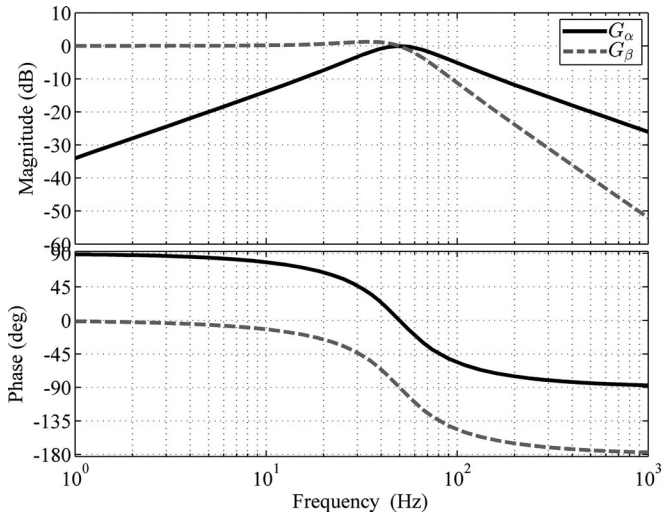

Fig. 3. Frequency response of $G_\alpha(s)$ and $G_\beta(s)$ for $k=1$.

II. Overview of FFSOGI-PLLs

A. First Topology

The first possible method for implementing the FFSOGI-PLL can be observed in Fig. 2 [10]. This structure, which is called the FFSOGI-PLL1, uses an FFSOGI-QSG in its input. The output signals of this FFSOGI-QSG can be described in the s-domain as

$$v_\alpha(s) = \overbrace{\frac{k\omega_n s}{s^2+k\omega_n s+\omega_n^2}}^{G_\alpha(s)} v(s) \tag{1}$$

$$v_\beta(s) = \overbrace{\frac{k\omega_n^2}{s^2+k\omega_n s+\omega_n^2}}^{G_\beta(s)} v(s). \tag{2}$$

Fig. 3 illustrates the frequency response of $G_\alpha(s)$ and $G_\beta(s)$ for $k=1$. It can be observed that $G_\alpha(s)$ and $G_\beta(s)$ keep their 90° phase difference under nominal and off-nominal grid frequencies. It implies that the outputs of the FFSOGI-QSG, i.e., v_α and v_β, are always orthogonal. These signals, however, are not in-phase and quadrature-phase with the single-phase input signal v under off-nominal frequencies. This issue results in a phase offset error in the PLL output. In the presence of small

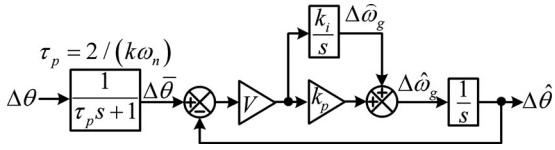

Fig. 4. Derived small-signal model for the FFSOGI-PLL1 in [10].

frequency drifts, this error is equal to

$$\angle G_\alpha(j\omega_g) \approx -\frac{\omega_g^2-\omega_n^2}{k\omega_n\omega_g}. \tag{3}$$

To correct this error, $\angle G_\alpha(j\omega_g)$ can be calculated using the frequency estimated by the PLL[1] and added (with an opposite sign) to its output [10]. It is worth noting that this idea (i.e., adding a phase-offset error compensator in the PLL output) has been widely used in designing different PLLs [12], [13].

On the other hand, it is clear from (4) and (5) that the output signals of the FFSOGI-QSG may not have the same amplitude under frequency drifts

$$|G_\alpha(j\omega_g)| = \frac{k\omega_n\omega_g}{\sqrt{\left(\omega_n^2-\omega_g^2\right)^2+\left(k\omega_n\omega_g\right)^2}} \tag{4}$$

$$|G_\beta(j\omega_g)| = \frac{k\omega_n^2}{\sqrt{\left(\omega_n^2-\omega_g^2\right)^2+\left(k\omega_n\omega_g\right)^2}}. \tag{5}$$

This fact is also noticeable from Fig. 3. This amplitude difference results in double-frequency oscillations in the estimated phase and frequency. To correct this difference, it is suggested in [10] to multiply the signal v_β by $\hat{\omega}_g/\omega_n$ or $\bar{\omega}_g/\omega_n$, where $\hat{\omega}_g$ and $\bar{\omega}_g$, as mentioned before, are estimations for the grid frequency. It is worth mentioning that a similar idea, but for a different QSG method, has already been proposed in [14].

Fig. 4 shows the model derived for the FFSOGI-PLL1 in [10], in which V is the grid voltage amplitude. Dynamics of the phase error compensator is neglected in this model. The theoretical analyses and the tuning procedure conducted in [10] are based on this model.

[1]The voltage-controlled oscillator input and the PI controller integrator output both provide estimations for the grid frequency. The latter one offers a higher filtering capability and, therefore, it is considered as the input signal of the phase error compensator in this letter.

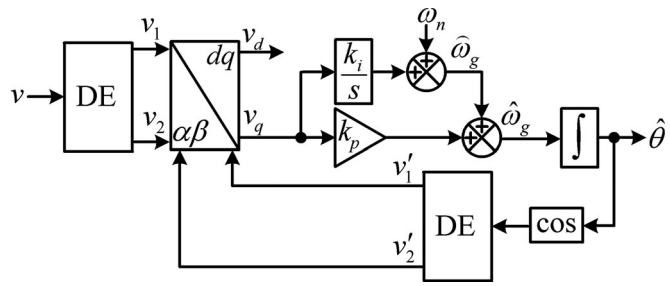

Fig. 5. Schematic diagram of the DE-PLL [11].

B. Second Topology

Fig. 5 illustrates the schematic diagram of a PLL called the derivative elements-based PLL (DE-PLL) [11]. Equations (6) and (7) describe the characteristic transfer functions of the DE

$$v_1(s) = \overbrace{\frac{\omega_n^2 s}{s^2 + k\omega_n s + \omega_n^2}}^{G_1(s)} v(s) \tag{6}$$

$$v_2(s) = \overbrace{\frac{\omega_n^2}{s^2 + k\omega_n s + \omega_n^2}}^{G_2(s)} v(s). \tag{7}$$

Comparing these equations with the characteristic transfer functions of the FFSOGI-QSG, i.e., (1) and (2), indicates that $G_1(s) = \omega_n G_\alpha(s)/k$ and $G_2(s) = G_\beta(s)/k$. Based on this fact, it is immediate to conclude that the DE-PLL is equivalent to the structure shown in Fig. 6, in which $k_p' = (w_n/k^2)k_p$ and $k_i' = (w_n/k^2)k_i$. Fig. 7 verifies this equivalence numerically. From now on, the structure shown in Fig. 6 is called the FFSOGI-PLL2. Restructuring the DE-PLL as the FFSOGI-PLL2 makes its understanding and its small-signal modeling easier.

In the FFSOGI-PLL2, as shown, only one trigonometric function is used and the second trigonometric function is created by using an FFSOGI-QSG. In this way, the same level of amplitude difference existing between v_α and v_β under frequency drifts is created between v_c and v_s. On the other hand, the same phase difference existing between v and v_α under off-nominal frequencies is generated between v and v_c, and the same nonorthogonality existing between v and v_β is created between v and v_s. In this way, some errors caused by the first FFSOGI-QSG in the PLL input are canaled by the second FFSOGI-QSG in the feedback path.

Fig. 8 shows the model derived for the FFSOGI-PLL2 (DE-PLL) in [11]. In this model, which is used for the tuning procedure and theoretical analyses in [11], dynamics of the FFSOGI-QSGs have been neglected.

III. Analysis of the FFSOGI-PLL1

A. Small-Signal Modeling

The model derived for the FFSOGI-PLL1 in [10] (see Fig. 4) does not take into account the dynamics of the output phase error compensator and, therefore, it is not accurate. Here, to achieve a more precise model, the phase error compensator is linearized and added to the model output.

Defining $\omega_g = \omega_n + \Delta\omega_g$ and substituting it into (3) gives

$$\angle G_\alpha(j\omega_g) \approx -\frac{\omega_n^2 + \Delta\omega_g^2 + 2\omega_n\Delta\omega_g - \omega_n^2}{k\omega_n^2 + k\omega_n\Delta\omega_g}$$

$$\approx -\frac{2}{k\omega_n}\Delta\omega_g = -\tau_p\Delta\omega_g. \tag{8}$$

Based on (8), Fig. 2, and Fig. 4, the accurate model of the FFSOGI-PLL1 can be obtained as shown in Fig. 9.

B. Parameter Tuning

The first design parameter is the constant k in the FFSOGI-QSG in the input of the FFSOGI-PLL1. As there is no feedback coupling between this FFSOGI-QSG and the rest of the system, tuning k and other parameters (the proportional and integral gains k_p and k_i) can be made separately. It is probably the main advantage of the FFSOGI-PLL1 over the standard SOGI-PLL.

From the characteristic transfer functions of the FFSOGI-QSG, i.e., (1) and (2), it is clear that $k = \sqrt{2}$ is corresponding to a damping factor of $1/\sqrt{2}$ and, therefore, it results in an optimal tradeoff between the settling time and overshoot of the FFSOGI-QSG during transients [15]. Hence, this value is selected here.

From Fig. 9, the closed-loop transfer function of the FFSOGI-PLL1 can be derived as

$$G_{cl}(s) = \frac{\Delta\hat{\theta}_c(s)}{\Delta\theta(s)} = \frac{1}{\tau_p s + 1}\frac{V\left(k_p + \tau_p k_i\right)s + V k_i}{s^2 + V k_p s + V k_i}. \tag{9}$$

By defining $k_p = 2\zeta\omega_n'/V$ and $k_i = (\omega_n')^2/V$, where ζ and ω_n' are the damping factor and natural frequency, respectively, and choosing proper values for ζ and ω_n', the FFSOGI-PLL1 proportional and integral gains can be determined. Here, $\zeta = 1/\sqrt{2}$ (which is corresponding to an optimum damping factor) and $\omega_n' = 2\pi 18$ rad/s are chosen. These selections result in $k_p = 159.9$ and $k_i = 12791$. In obtaining these values, $V = 1$ p.u. is assumed.

C. Comparison With the Standard SOGI-PLL

In the standard SOGI-PLL, there is a feedback coupling between the SOGI-QSG and the rest of the system. Based on this fact and the small-signal model of the standard SOGI-PLL (see [8, Fig. 6]), it can be concluded that the parameter k in the SOGI-PLL should be as large as possible to achieve a fast dynamic response. In [8], a value around 2 is recommended. Therefore, $k = 2$ is selected here. The proportional and integral gains of the standard SOGI-PLL can now be selected using the symmetrical optimum method, as suggested in [8]. The obtained values are $k_p = 130.1$ and $k_i = 7014$.

To ensure that the condition of comparison is fair, the closed-loop frequency response of the FFSOGI-PLL1 and the standard SOGI-PLL are compared in Fig. 10. These frequency responses are obtained using the closed-loop transfer function of the FFSOGI-PLL1 [i.e., (9)] and that of the standard SOGI-PLL, which can be found in [8]. As can be seen in Fig. 10, both PLLs have almost the same closed-loop bandwidth, which

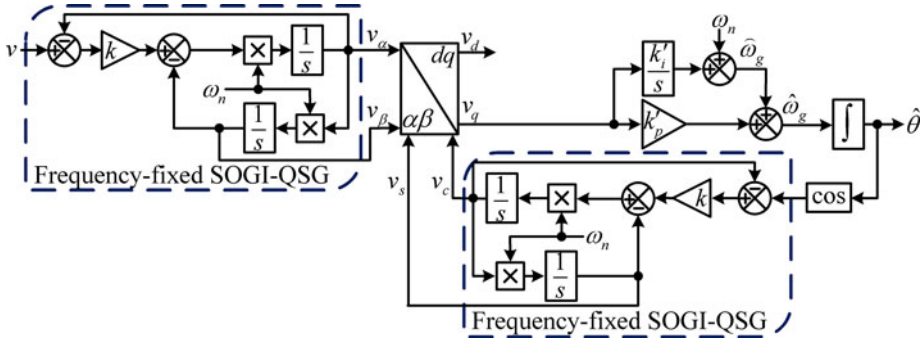

Fig. 6. Schematic diagram of the FFSOGI-PLL2. This structure, as far as the phase/frequency estimation is concerned, is mathematically equivalent to the DE-PLL.

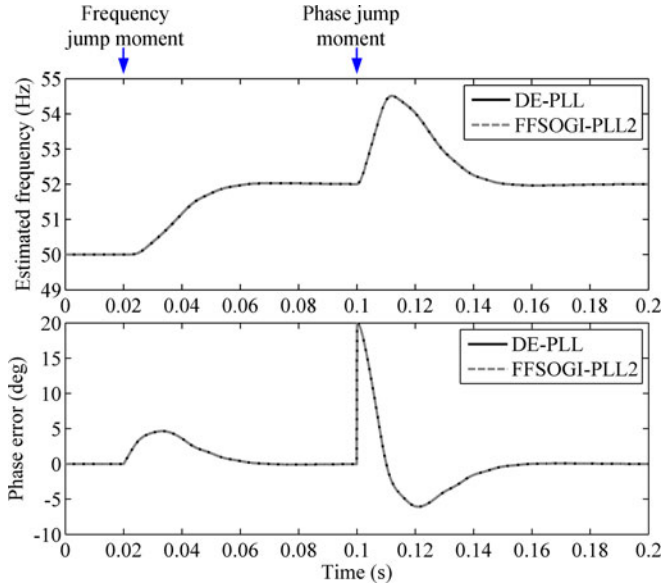

Fig. 7. Numerical performance comparison between the DE-PLL and FFSOGI-PLL2 under a +2 Hz frequency jump and a $+20^\circ$ phase jump. DE-PLL Parameters: $k = 2$, $k_p = 1.657$, $k_i = 89.3$. FFSOGI-PLL2 parameters: $k = 2$, $k_p' = (w_n/k^2)k_p = 130.1$, and $k_i' = (w_n/k^2)k_i = 7014$.

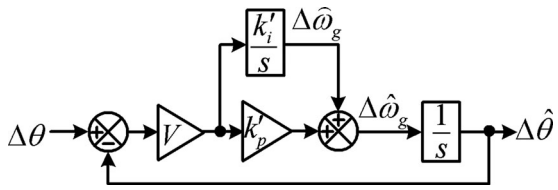

Fig. 8. Derived small-signal model for the FFSOGI-PLL2 (DE-PLL) in [11].

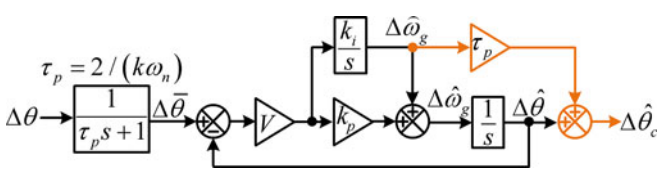

Fig. 9. Accurate small-signal model of the FFSOGI-PLL1.

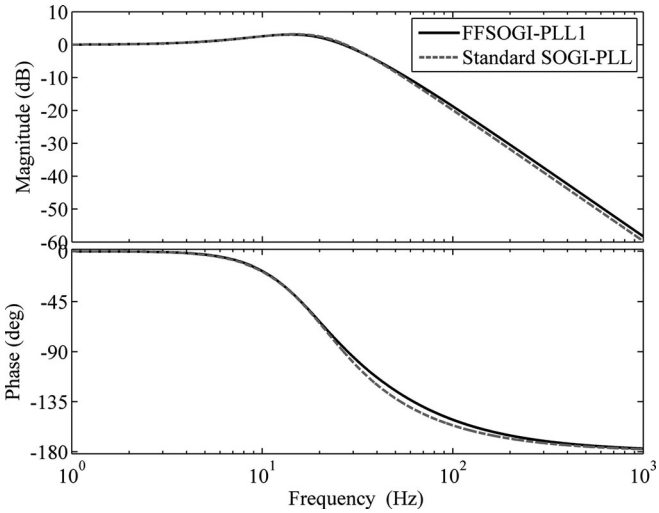

Fig. 10. Closed-loop frequency response of the FFSOGI-PLL1 and the standard SOGI-PLL.

implies the selected control parameters ensure a fair condition for the comparison.

Three tests are defined:

1) Test 1: a frequency jump of $+2$ Hz in the grid voltage happens;
2) Test 2: the grid voltage is distorted with low-order harmonics, the total harmonic distortion of the grid voltage in this test is around 8.25%;
3) Test 3: the grid voltage contains a 0.05 p.u. dc component.

The obtained results are shown in Fig. 11. These results have been obtained using the dSPACE 1006 platform. The sampling frequency is 10 kHz throughout the experimental studies. As can be seen in Fig. 11(a) and (b), the FFSOGI-PLL1 and the standard SOGI-PLL have a close dynamic response and harmonic filtering capability (the harmonic rejection of the standard SOGI-PLL is slightly better). However, from the dc offset rejection point of view, the FFSOGI-PLL1 offers a better performance. The reason is that the damping factor k in the FFSOGI-PLL1 is smaller than that in the standard SOGI-PLL. For more details, refer to [16] and [17].

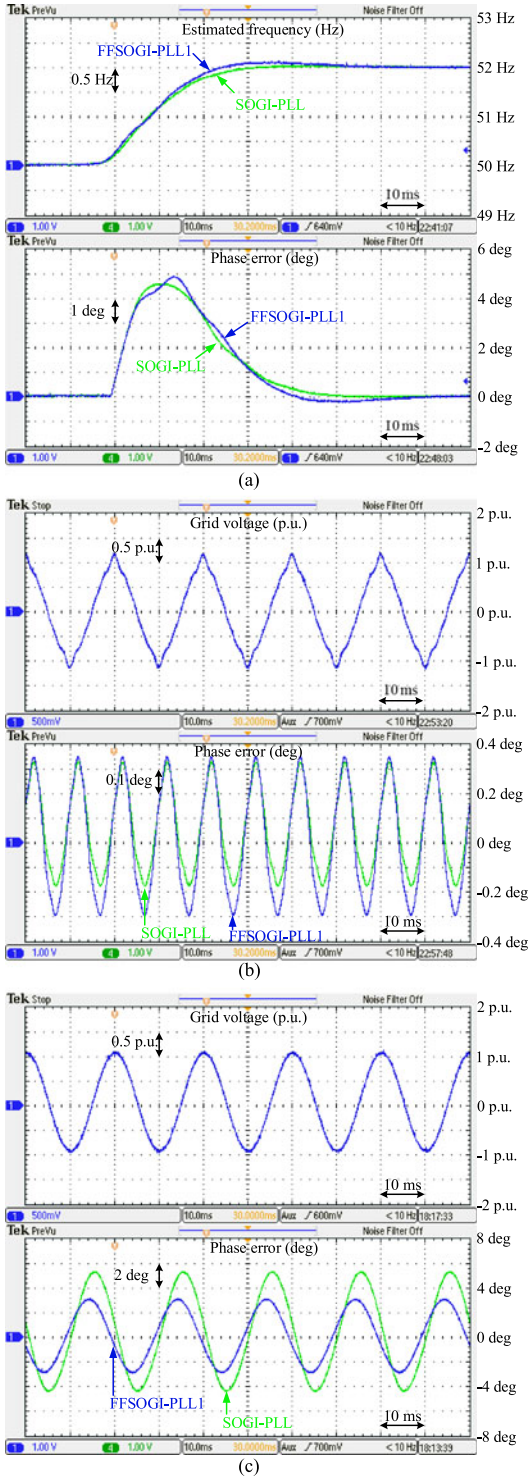

Fig. 11. Performance comparison between the FFSOGI-PLL1 and standard SOGI-PLL under: (a) test 1, (b) test 2, and (c) test 3.

IV. Analysis of the FFSOGI-PLL2 (DE-PLL)

A. Small-Signal Modeling

In the modeling of the FFSOGI-PLL2 (DE-PLL) in [11], dynamics of the FFSOGI-QSGs are neglected. In what follows, a more accurate modeling of the FFSOGI-PLL2 is presented.

Assume that the single-phase input signal of the FFSOGI-PLL2 is

$$v(t) = V\cos\underbrace{(\omega_g t)}_{\theta} \tag{10}$$

where V, θ, and ω_g denote the amplitude, phase angle, and angular frequency, respectively.

Considering (1), (2), and (10), and assuming that $k < 2$, the output signals of the first FFSOGI-QSG in the FFSOGI-PLL2, i.e., v_α and v_β, can be expressed as

$$\begin{aligned} v_\alpha(t) = {} & VA_{\alpha_1}\cos\left(\sqrt{1-k^2/4}\,\omega_n t+\varphi_{\alpha_1}\right)e^{-\frac{k\omega_n t}{2}} \\ & + VA_{\alpha_2}\cos(\theta+\varphi) \end{aligned} \tag{11}$$

$$\begin{aligned} v_\beta(t) = {} & VA_{\beta_1}\sin\Big(\overbrace{\sqrt{1-k^2/4}\,\omega_n t}^{\theta_k}+\varphi_{\beta_1}\Big)e^{-\frac{k\omega_n t}{2}} \\ & + VA_{\beta_2}\sin(\theta+\varphi) \end{aligned} \tag{12}$$

where A_{α_1}, A_{α_2}, A_{β_1}, A_{β_2}, φ_{α_1}, φ_{β_1}, and φ are all functions of k, ω_n, and ω_g. The definition of these parameters is not presented as it does not matter in the modeling procedure. The only required information is that A_{α_2} and A_{β_2} are equal to (close to) one when ω_g is equal to (close to) ω_n.

Under a quasi-locked state, the output signals of the second FFSOGI-QSG in the FFSOGI-PLL2, i.e., v_c and v_s, can be approximated by

$$v_c(t) \approx A_{\alpha_1}\cos(\theta_k+\varphi_{\alpha_1})e^{-\frac{k\omega_n t}{2}} + A_{\alpha_2}\cos(\hat{\theta}+\varphi) \tag{13}$$

$$v_s(t) \approx A_{\beta_1}\sin(\theta_k+\varphi_{\beta_1})e^{-\frac{k\omega_n t}{2}} + A_{\beta_2}\sin(\hat{\theta}+\varphi). \tag{14}$$

Using (11)–(14), the signal v_q (the PI controller input signal) in the FFSOGI-PLL2 can be expressed as

$$\begin{aligned} v_q(t) = {} & -v_s(t)v_\alpha(t)+v_c(t)v_\beta(t) \\ \approx {} & V\Big[-A_{\alpha_2}A_{\beta_2}\sin(\hat{\theta}+\varphi)\cos(\theta+\varphi) \\ & - A_{\alpha_1}A_{\beta_2}\sin(\hat{\theta}+\varphi)\cos(\theta_k+\varphi_{\alpha_1})e^{-\frac{k\omega_n t}{2}} \\ & - A_{\alpha_2}A_{\beta_1}\cos(\theta+\varphi)\sin(\theta_k+\varphi_{\beta_1})e^{-\frac{k\omega_n t}{2}} \\ & - A_{\alpha_1}A_{\beta_1}\cos(\theta_k+\varphi_{\alpha_1})\sin(\theta_k+\varphi_{\beta_1})e^{-k\omega_n t} \\ & + A_{\alpha_2}A_{\beta_2}\sin(\theta+\varphi)\cos(\hat{\theta}+\varphi) \\ & + A_{\alpha_1}A_{\beta_2}\sin(\theta+\varphi)\cos(\theta_k+\varphi_{\alpha_1})e^{-\frac{k\omega_n t}{2}} \\ & + A_{\alpha_2}A_{\beta_1}\cos(\hat{\theta}+\varphi)\sin(\theta_k+\varphi_{\beta_1})e^{-\frac{k\omega_n t}{2}} \\ & + A_{\alpha_1}A_{\beta_1}\cos(\theta_k+\varphi_{\alpha_1})\sin(\theta_k+\varphi_{\beta_1})e^{-k\omega_n t}\Big]. \end{aligned} \tag{15}$$

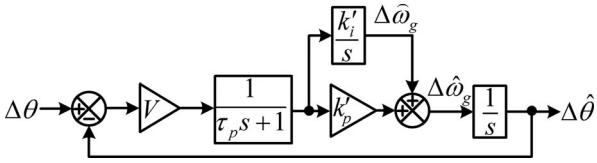

Fig. 12. Accurate model of the FFSOGI-PLL2.

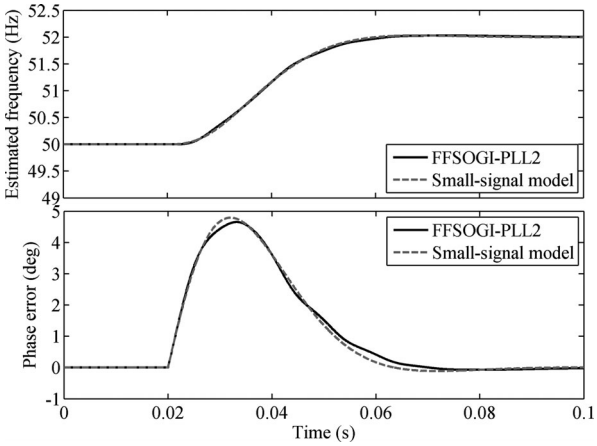

Fig. 13. Accuracy assessment of the model shown in Fig. 12. Parameters: $k = 2$, $k_p' = 130.1$, and $k_i' = 7014$.

Using basic trigonometric identities and applying some simple mathematical manipulations to (15) gives

$$v_q(t) \approx V \overbrace{A_{\alpha_2} A_{\beta_2}}^{\approx 1} \overbrace{\sin(\theta - \hat{\theta})}^{\approx(\Delta\theta - \Delta\hat{\theta})} + V \left[A_{\alpha_1} A_{\beta_2} \left\{ \sin(\theta + \varphi) - \sin(\hat{\theta} + \varphi) \right\} \cos(\theta_k + \varphi_{\alpha_1}) - A_{\alpha_2} A_{\beta_1} \left\{ \cos(\theta + \varphi) - \cos(\hat{\theta} + \varphi) \right\} \sin(\theta_k + \varphi_{\beta_1}) \right] e^{-\frac{k\omega_n t}{2}}. \quad (16)$$

According to (16), the oscillatory terms decay to zero with a time constant $\tau_p = 2/(k\omega_n)$ and v_q converges to $V(\Delta\theta - \Delta\hat{\theta})$. Therefore, dynamics of the signal v_q in the Laplace domain can be approximated by

$$v_q(s) = V \frac{1}{\tau_p s + 1} [\Delta\theta(s) - \Delta\hat{\theta}(s)]. \quad (17)$$

Based on (17) and the structure of the FFSOGI-PLL2 (see Fig. 6), the model shown in Fig. 12 can be derived for the FFSOGI-PLL2. Notice that, in obtaining this model, $k < 2$ was assumed. Despite this fact, it can be proved that this model is also accurate outside this range, i.e., when k is equal to (or very slightly larger than) 2.

The model of the FFSOGI-PLL2 is exactly the same as that of the standard SOGI-PLL (see [8, Fig. 6]). It means that the FFSOGI-PLL2 and the standard SOGI-PLL (as far as the frequency/phase estimation is concerned) are equivalent systems, at least from the small-signal point of view. This equivalence also implies that the same tuning procedure as that of the standard SOGI-PLL is applicable to the FFSOGI-PLL2.

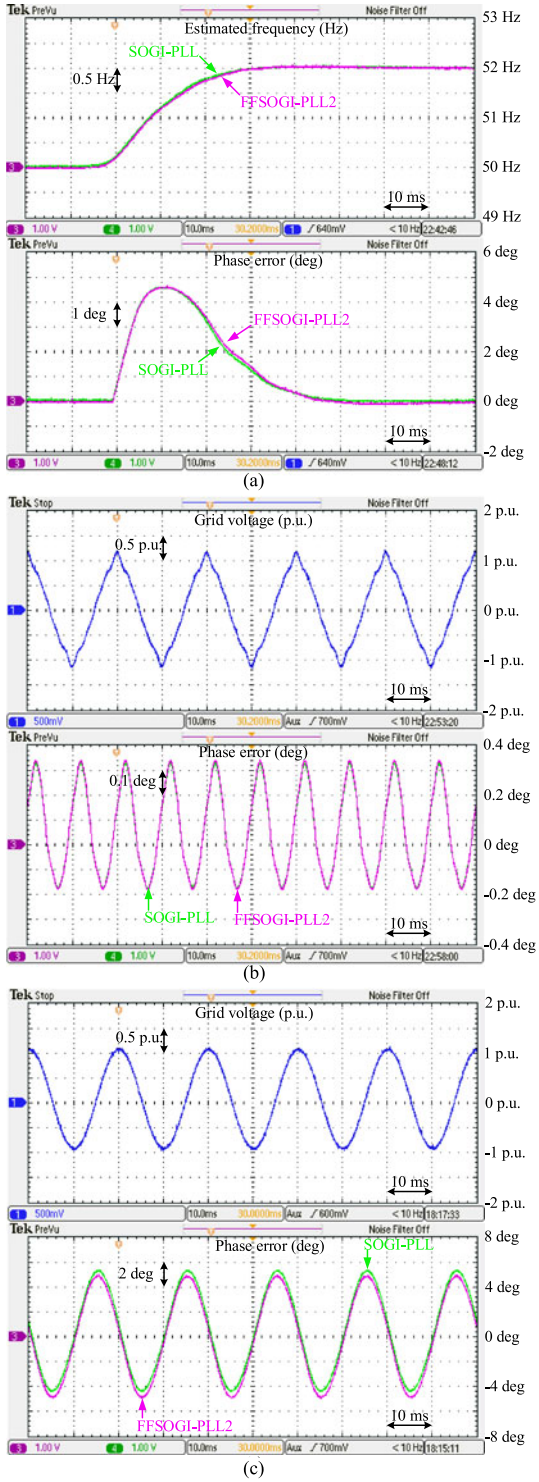

Fig. 14. Performance comparison between the FFSOGI-PLL2 and standard SOGI-PLL under: (a) test 1, (b) test 2, and (c) test 3.

The tuning procedure of the standard SOGI-PLL has been already discussed in detail in [8]. Hence, it is not repeated here.

The accuracy assessment of the model illustrated in Fig. 12 is carried out using a +2-Hz frequency jump test. The obtained results, which are shown in Fig. 13, demonstrate that the model is quite accurate.

B. Comparison With the Standard SOGI-PLL

The same tests used in Section III-C are considered here. The control parameters of the standard SOGI-PLL are also the same as before, i.e., $k = 2$, $k_p = 130.1$, and $k_i = 7014$. As the FFSOGI-PLL2 and the standard SOGI-PLL have identical models, then the same parameters as those of the standard SOGI-PLL are used for the FFSOGI-PLL2. The obtained results are shown in Fig. 14. It can be observed that the FFSOGI-PLL2 and the standard SOGI-PLL have almost identical results which confirm their equivalence.

V. Conclusion

In this letter, the accurate modeling of two FFSOGI-PLLs was presented. These models make finding a fair condition of comparison with the standard SOGI-PLL possible. A performance comparison between these FFSOGI-PLLs and the standard SOGI-PLL under a fair condition was then conducted. The theoretical and experimental findings prove that the FFSOGI-PLL2 and the standard SOGI-PLL (as far as the frequency/phase estimation is concerned) are practically equivalent. Regarding the FFSOGI-PLL1, the experimental results demonstrate no advantage over the standard SOGI-PLL from the dynamic response and harmonic filtering capability points of view. From the perspective of the dc-offset rejection ability, nevertheless, the FFSOGI-PLL1 offers a better performance. Although not shown in this letter to save the space, it should be mentioned here that the FFSOGI-PLL1 and FFSOGI-PLL2 (DE-PLL), contrary to the standard SOGI-PLL, cannot accurately estimate the grid voltage amplitude under off-nominal frequencies.

References

[1] S. Golestan, J. M. Guerrero, and J. C. Vasquez, "Single-phase PLLs: A review of recent advances," *IEEE Trans. Power Electron.*, to be published, 2017.

[2] R. M. S. Filho, P. F. Seixas, P. C. Cortizo, L. A. B. Torres, and A. F. Souza, "Comparison of three single-phase PLL algorithms for UPS applications," *IEEE Trans. Ind. Electron.*, vol. 55, no. 8, pp. 2923–2932, Aug. 2008.

[3] S. Golestan, M. Ramezani, J. M. Guerrero, F. D. Freijedo, and M. Monfared, "Moving average filter based phase-locked loops: Performance analysis and design guidelines," *IEEE Trans. Power Electron.*, vol. 29, no. 6, pp. 2750–2763, Jun. 2014.

[4] A. Elrayyah, Y. Sozer, and M. Elbuluk, "Robust phase locked-loop algorithm for single-phase utility-interactive inverters," *IET Power Electron.*, vol. 7, no. 5, pp. 1064–1072, May 2014.

[5] I. Carugati, P. Donato, S. Maestri, D. Carrica, and M. Benedetti, "Frequency adaptive PLL for polluted single-phase grids," *IEEE Trans. Power Electron.*, vol. 27, no. 5, pp. 2396–2404, May 2012.

[6] S. Golestan, M. Monfared, F. D. Freijedo, and J. M. Guerrero, "Design and tuning of a modified power-based PLL for single-phase grid-connected power conditioning systems," *IEEE Trans. Power Electron.*, vol. 27, no. 8, pp. 3639–3650, Aug. 2012.

[7] M. Karimi-Ghartemani, "A unifying approach to single-phase synchronous reference frame PLLs," *IEEE Trans. Power Electron.*, vol. 28, no. 10, pp. 4550–4556, Oct. 2013.

[8] S. Golestan, M. Monfared, F. D. Freijedo, and J. M. Guerrero, "Dynamics assessment of advanced single-phase PLL structures," *IEEE Trans. Ind. Electron.*, vol. 60, no. 6, pp. 2167–2177, Jun. 2013.

[9] M. Ciobotaru, R. Teodorescu, and F. Blaabjerg, "A new single-phase PLL structure based on second order generalized integrator," in *Proc. 2006 37th IEEE Power Electron. Spec. Conf.*, Jun. 2006, pp. 1–6.

[10] F. Xiao, L. Dong, L. Li, and X. Liao, "A frequency-fixed SOGI-based PLL for single-phase grid-connected converters," *IEEE Trans. Power Electron.*, vol. 32, no. 3, pp. 1713–1719, Mar. 2017.

[11] Q. Guan, Y. Zhang, Y. Kang, and J. M. Guerrero, "Single-phase phase-locked loop based on derivative elements," *IEEE Trans. Power Electron.*, vol. 32, no. 6, pp. 4411–4420, Jun. 2017.

[12] S. Golestan, F. D. Freijedo, A. Vidal, A. G. Yepes, J. M. Guerrero, and J. Doval-Gandoy, "An efficient implementation of generalized delayed signal cancellation PLL," *IEEE Trans. Power Electron.*, vol. 31, no. 2, pp. 1085–1094, Feb. 2016.

[13] S. Golestan, J. M. Guerrero, A. Vidal, A. G. Yepes, J. Doval-Gandoy, and F. D. Freijedo, "Small-signal modeling, stability analysis and design optimization of single-phase delay-based PLLs," *IEEE Trans. Power Electron.*, vol. 31, no. 5, pp. 3517–3527, May 2016.

[14] C. Subramanian and R. Kanagaraj, "Single-phase grid voltage attributes tracking for the control of grid power converters," *IEEE J. Emerg. Sel. Topics Power Electron.*, vol. 2, no. 4, pp. 1041–1048, Dec. 2014.

[15] R. Teodorescu, M. Liserre, and P. Rodriguez, *Grid Converters for Photovoltaic and Wind Power Systems*. Hoboken, NJ, USA: Wiley, 2011, pp. 43–91.

[16] S. Lubura, M. Soja, S. Lale, and M. Ikic, "Single-phase phase locked loop with dc offset and noise rejection for photovoltaic inverters," *IET Power Electron.*, vol. 7, no. 9, pp. 2288–2299, Sep. 2014.

[17] M. Karimi-Ghartemani, S. A. Khajehoddin, P. K. Jain, A. Bakhshai, and M. Mojiri, "Addressing DC component in PLL and notch filter algorithms," *IEEE Trans. Power Electron.*, vol. 27, no. 1, pp. 78–86, Jan. 2012.